Self-consistent modelling of self-organized patterns of spots on anodes of DC glow discharges

M. S. Bieniek, P. G. C. Almeida, and M. S. Benilov[a]
Departamento de Física, Faculdade de Ciências Exatas e da Engenharia, Universidade da Madeira, Largo do Município, 9000 Funchal, Portugal, and
Instituto de Plasmas e Fusão Nuclear, Instituto Superior Técnico, Universidade de Lisboa, 1041 Lisboa, Portugal
[a] email *benilov@uma.pt*

Abstract

Self-organized patterns of spots on a flat metallic anode in a cylindrical glow discharge tube are simulated. A standard model of glow discharges is used, comprising conservation and transport equations for a single species of ion and electrons, written with the use of the drift-diffusion and local-field approximations, and the Poisson equation. Only processes in the near-anode region are considered and the computation domain is the region between the anode and the discharge column. Multiple solutions, existing in the same range of discharge current and describing modes with and without anode spots, are computed for the first time. A reversal of the local anode current density in the spots was found, i.e. mini-cathodes are formed inside the spots or, as one could say, anode spots operate as a unipolar glow discharge. The solutions do not fit into the conventional pattern of self-organization in bistable nonlinear dissipative systems; e.g. the modes are not joined by bifurcations.

1 Introduction

For more than a century now beautiful self-organized patterns have been observed on both solid and liquid anodes of DC glow discharges, [1–8] and [9, 10], respectively. A question arises as to what mechanism is responsible for this self-organization. Another question is to what extent are these patterns similar to self-organized patterns observed on solid [11–22] and liquid [23, 24] cathodes of dc glow discharges. An additional interest in the physics of self-organization on anodes of glow discharges has developed recently, when

it has been shown that self-organized patterns on liquid anodes of atmospheric pressure glow microdischarges reveal a nontrivial cancer-inhibiting capability [25].

There is a number of publications dedicated to different kinds of spots and spot patterns on anodes of gas discharges. Patterns of spots have been simulated by means of a phenomenological approach based on the general trends of self-organization in [6]. Numerical simulations of glow discharges have revealed current density stripes on anodes [26], a circular spot [27], and a circular spot surrounded by a ring [27]. A theoretical analysis, and experimental investigation, of the anode glow layer region performed in [28] indicate that instabilities found in the so-called subnormal regime are a precursor for the formation of anode spots. Also in [28], the effect that the spots produce on the homogeneity of the plasma column is investigated. Spot patterns on anodes of low-current low-pressure arc discharges have been observed in [29, 30]. Diffuse, constricted, and multiple-spot modes are observed on anodes of high-pressure arc discharges [31–36] and impressive results have been achieved in time-dependent 3D numerical simulations of the multiple-spot mode [37, 38]. Various types of double layer structures and the so-called plasma balls, that form on a small anode in contact with a low-pressure plasma and sometimes are also termed anode spots, have been studied experimentally and theoretically [39–46]. Unfortunately, the questions concerning the mechanism of self-organization on glow anodes, mentioned in the preceding paragraph, remain unanswered.

Self-organized arrangements of spots and patterns on cathodes of DC arc and glow discharges have been understood and systematically described in terms of multiple steady-state solutions, which exist in conventional models of arc and glow discharges over the same range of discharge current and describe modes associated with different cathode spots and cathode spot patterns; e.g., [47] and references therein. We hypothesize that the same approach is applicable to spots and spot patterns on anodes of DC glow discharges. In other words, we postulate that spots and spot patterns on anodes of DC glow discharges can be described by a new class of solutions, that exist in conventional models of glow discharges, alongside the solution associated with the spotless mode of current transfer. In this work we prove this hypothesis. Two solutions, as examples, are computed over the same, wide, range of current. One solution describes an axially symmetric diffuse, or spotless, mode, and the other solution describes a three-dimensional mode with azimuthal periodicity comprising a self-organized pattern of 8 anode spots.

The outline of the paper is as follows. The model is described in section 2. In section 3, results of the modelling are given and discussed. Conclusions are drawn in section 4.

2 The model

Consider a cylindrical DC glow discharge tube that is long enough that the effect of the electrodes become obviated in the column. In the column the density of charged species and electric field are independent of the axial coordinate. This invariance allows us to choose an asymptotically accurate set of boundary conditions on a domain that contains only the region from the anode to the column; figure 1. The computation domain is adequate for an investigation of anode spots, or patterns of spots, appearing as a result of processes of plasma-anode interaction only.

The simplest model of a glow discharge is used, which is well-known but briefly summarized here for completeness. It comprises equations of conservation of electrons and a

single ion species, the transport equations, written in the drift-diffusion approximation, and Poisson's equation:

$$\begin{aligned}
\frac{\partial n_i}{\partial t} + \nabla \cdot \mathbf{J}_i &= n_e\,\alpha\,\mu_e\,E - \beta\,n_e\,n_i, \quad \mathbf{J}_i = -D_i\,\nabla n_i - n_i\,\mu_i\,\nabla\varphi, \\
\frac{\partial n_e}{\partial t} + \nabla \cdot \mathbf{J}_e &= n_e\,\alpha\,\mu_e\,E - \beta\,n_e\,n_i, \quad \mathbf{J}_e = -D_e\,\nabla n_e + n_e\,\mu_e\,\nabla\varphi, \\
\varepsilon_0\,\nabla^2\varphi &= -e\,(n_i - n_e)\,.
\end{aligned} \tag{1}$$

Here n_i, n_e, $\mathbf{J}_i$, $\mathbf{J}_e$, D_i, D_e, μ_i, and μ_e are number densities, densities of transport fluxes, diffusion coefficients, and mobilities of the ions and electrons, respectively; α is Townsend's ionization coefficient; β is coefficient of dissociative recombination; φ is electrostatic potential, $E = |\nabla\varphi|$ is electric field strength; ε_0 is permittivity of free space; and e is elementary charge. The local-field approximation is employed, i.e., electron transport and kinetic coefficients are assumed to depend on the local electric field only.

Let us introduce cylindrical coordinates (r, ϕ, z) with the z-axis in line with the axis of the discharge tube; figure 1. The computation domain is $\{0 \le r \le R, 0 \le z \le h\}$, where R is the tube radius and the boundary $z = h$ is positioned in the discharge column.

Standard boundary conditions are used for the lateral dielectric wall, $r = R$, describing absorption of ions and electrons (as in e.g., [48, 49]) and the surface charge accumulation:

$$J_{in} = \sqrt{\frac{8k_BT_i}{\pi m_i}}\frac{n_i}{4}, \quad J_{en} = \sqrt{\frac{8k_BT_e}{\pi m_e}}\frac{n_e}{2}, \tag{2}$$

$$-\varepsilon_0\frac{\partial\varphi}{\partial n} = \rho_s, \quad \frac{\partial\rho_s}{\partial t} = e\,(J_{in} - J_{en})\,. \tag{3}$$

Here subscript n represents the projection of the corresponding vector along n the normal directed outside the computation domain, ρ_s is surface charge density, T_i and T_e are ion and electron temperatures (known parameters), m_i and m_e are the ion and electron masses, and k_B is Boltzmann's constant. When a steady-state has been reached, the surface charge accumulation equation, second equation (3), becomes equivalent to the electrical insulation condition, $J_{in} - J_{en} = 0$.

Boundary conditions at the anode surface ($z = 0$) are

$$J_{in} = \sqrt{\frac{8k_BT_i}{\pi m_i}}\frac{n_i}{4}, \quad J_{en} = \sqrt{\frac{8k_BT_e}{\pi m_e}}\frac{n_e}{2} - \delta_a\gamma J_{in}, \quad \varphi = 0. \tag{4}$$

Here δ_a is the step function, $\delta_a = 1$ if $E_z < 0$ (i.e., the local electric field is directed to the anode) and $\delta_a = 0$ if $E_z > 0$. The first and second boundary conditions (4) are similar to the ones for the dielectric wall (2), except for the second term on the right-hand side of the boundary condition for the electrons (the second equation in (4)). This term describes secondary electron emission, which may become relevant if the local electric field is directed from the plasma to the anode.

Note that the choice of which secondary electron emission coefficient, γ, to use was not clear as the anode sheath voltage and, consequently, the energy of incident ions are small. In any case, this term produces a small effect even for γ of order unity, since its magnitude for comparable n_i and n_e is of the order of $\gamma\sqrt{m_eT_i/(m_iT_e)}$ with respect to

the first term on the right-hand side of the second equation in (4). The third condition in (4) defines the zero of potential.

The boundary $z = h$ is positioned in the discharge column, where the charged species densities are independent of ϕ, z and the axial electric field is constant (independent of r, ϕ, z):

$$\frac{\partial n_i}{\partial z} = 0, \quad \frac{\partial n_e}{\partial z} = 0, \quad \frac{\partial \varphi}{\partial z} = -E_z. \tag{5}$$

Here E_z is the axial electric field; a given parameter which may be chosen to ensure a desired value of the discharge current I. The parameter h has to be large enough so the conditions (5) are satisfied not just at the boundary $z = h$, but also in a region adjacent to the boundary; in other words, h has to be larger than the thickness of the near-anode region.

We hypothesize that the problem (1)-(5) admits an axially symmetric (2D) steady-state solution, describing a spotless, or diffuse, mode of current transfer to the anode, and three-dimensional steady-state solutions, presumably describing modes with patterns of spots. By analogy with computed spot patterns on cathodes of DC glow discharges, and in qualitative agreement with experimental results on anode spot patterns, we assume that the 3D solutions are periodic in ϕ with the period $2\pi/n$, where $n = 1, 2, 3, \ldots$, then it is sufficient to limit the computation domain to a half-period of the desired 3D solution: $0 \le \phi \le \pi/n$. Boundary conditions at $\phi = 0$ (plane $ABED$ in figure 1) and $\phi = \pi/n$ (plane $ACFD$) are zero normal derivatives,

$$\frac{\partial n_i}{\partial n} = 0, \quad \frac{\partial n_e}{\partial n} = 0, \quad \frac{\partial \varphi}{\partial n} = 0, \tag{6}$$

so that $\phi = 0$ and $\phi = \pi/n$ represent planes of symmetry of the solution considered.

Results reported in this work refer to a low-pressure discharge in helium, which was the plasma-producing gas in the experiment [2]. The competing requirements of reducing the volume of the computation domain and resolving both the near-anode region and the adjacent part of the discharge column determined the final choice of the domain and pressure: the discharge tube radius was $R = 0.5\,\mathrm{mm}$, the height of the computation domain was $h = 5\,\mathrm{mm}$, and the pressure was 5 Torr. The (only) ionic species considered is He_2^+. The transport and kinetic coefficients are the same as in [50], with $\gamma = 0.03$, $T_e = 1\,\mathrm{eV}$, and $T_i = 300\,\mathrm{K}$.

The modelling was performed by means of the Plasma Module of COMSOL Multiphysics, supplemented with residual-based stabilization. Both the steady-state and time-dependent forms of problem (1)-(6) have been solved. The former was made possible by adapting the Plasma Module so that it could be used in combination with a stationary solver.

3 Results and discussion

One of the computed solutions reported in this paper is axially symmetric (2D) and describes the spotless mode. As an example of a non-axisymmetric (3D) mode, the mode with $n = 8$ is reported, which describes a mode with eight spots. Note that the relatively high value of n permits a relatively small computation domain and thus reduces the required RAM and computation time.

The 2D solution was computed in a standard way by means of a stationary solver. It has been found in this work that 3D solutions do not bifurcate from the 2D solution, in contrast to solutions describing cathodic spots and patterns of spots in arc and glow cathodes, which do bifurcate from a fundamental (generally 2D) solution. Therefore the approach developed for the systematic computation of multiple solutions describing spots and patterns on cathodes of arc and DC glow discharges [47] could not be used. To find the 3D solution reported in this work, we first solved the z-independent, axially symmetric, and steady-state form of the problem (1), (2) supplemented with the electrical insulation condition, describing the discharge column. (Analytical solutions of this 1D problem for the limiting cases corresponding to free and ambipolar diffusion [51] and a recombination-dominated discharge were used to validate the code.) In order to obtain the 3D solution, a solution of the 1D problem governing the column for the discharge current $I = 10\,\mathrm{mA}$ was introduced as an initial condition for the time-dependent solver, the one solving the time-dependent form of the problem (1)-(6) including surface charge accumulation at the dielectric wall, equation (3). The computations have been performed with the value of E_z, the input parameter describing the axial electric field in the column, corresponding to the $I = 30\,\mathrm{mA}$, and not to 10 mA. The time-dependent solver was ran; the mismatch in E_z introduced a perturbation to the system that resulted in an evolution to a 3D time-independent solution to the problem. (Note that other perturbations were used, however, most would result in the loss of computational stability. A systematic investigation of different perturbations which could eventually lead to patterns of other types would be interesting and may be addressed in the future.) The stationary solver was then used to compute the 3D solution in a wide range of current.

3.1 Current-voltage characteristics of the anode region

Consider the potential distribution in the discharge column, φ_c, (which is axially symmetric),

$$\varphi_c\,(r,z) = -(z-h)E_z + \varphi_h\,(r)\,, \tag{7}$$

where $\varphi_h\,(r)$ is the distribution of potential at the computational boundary, $z = h$. We define the near-anode voltage drop as the difference between the potential at the anode (equal to zero), and the potential that is obtained by extrapolation of the column solution (7) to the anode ($z = 0$):

$$U = -hE_z - \varphi_h\,(r)\,. \tag{8}$$

Note the second term on the right-hand side of this definition depends on r. In order to remove the dependence on r and find an integral characteristic, one has, for example, to evaluate the right-hand side of equation (8) on the axis, or edge, of the discharge tube, or take an average value over the cross section. However, whatever choice is made is irrelevant in so far as a graphical representation of multiple solutions is concerned: different solutions with the same discharge current will coincide in the column to the accuracy of a shift of potential by a constant. Therefore, whatever way is chosen to evaluate the right-hand side of equation (8), as long as it is the same for different solutions, the difference in U between the different solutions will be equal. We indicate for definiteness that in this work the right-hand side of equation (8) is evaluated on the axis.

Shown in Figure 2 are near-anode current-voltage characteristics (CVCs) of two solutions, existing in the same range of current. One solution describes a 3D mode that is azimuthally periodic, the other a 2D mode that is axially symmetric. The 3D mode has a negative value of the near-anode voltage in the range of currents investigated, while the 2D mode has a positive value of the near-anode voltage in the investigated current range.

It is of interest to compare the CVCs in figure 2 to the computed CVCs of DC glow discharges with self-organized cathode spots (e.g., figure 3 of [52]). In the case of the cathode spots there is an N-shaped CVC corresponding to the 2D solution, with the CVC corresponding to the 3D solutions branching off on the falling section of the CVC of the 2D solution; as per the general pattern of self-organization in bistable nonlinear dissipative systems with a positive feedback. The CVCs shown in figure 2 are very different: no pronounced N-shaped CVC was found for the 2D solution, and no bifurcations were found in a wide current range.

3.2 Anode spot structure

The electron number density on the surface of the anode for the 3D mode at 10 mA is shown in figure 3. Electron density is organized in an azimuthally periodic pattern of spots. The pattern is similar to that observed experimentally [2, Figure 2].

Densities of ions and electrons and the potential distribution are shown in figure 4 in the plane of symmetry $\phi = 0$ (in the longitudinal cross section $ABED$ passing through the tube axis and the centre of a spot) for $I = 1$ mA.

The distribution of the charged particle densities along the axial direction from the centre of a spot towards the column (line GH), at $I = 0.1$ mA and 35 mA, are shown in figure 5. There is a region with $n_i > n_e$, i.e., an ion sheath, adjacent to the electrode. The ion densities in the sheath are of the same order of magnitude for the two discharge currents, while the densities of the charged particles in the column vary by more than an order of magnitude. For $I = 0.1$ mA, charge separation is seen also in the column, which is due to diffusion coming into play near the (absorbing) lateral wall.

The distribution of the electric field for $I = 35$ mA is shown in figure 5. The electric field in the ion sheath is two orders of magnitude greater than that in the quasi-neutral region. The former points towards the anode, while the latter points away from the anode. Note that field reversals have previously been observed near cold anodes of arc discharges [36, 53, 54], although not in connection with self-organized anode spots.

It is seen in figure 4 c) that in the spot the potential of the adjacent plasma is above the electrode potential, and it is seen from figure 5 that quasi-neutral plasma is extended close, up to 1 μm, to the electrode. It is seen from figure 4 c) that the potential of the adjacent plasma is below the electrode potential at large distances from the spot; skipping for brevity results on the charge particle distribution, we only note that there is an electron sheath adjacent to the electrode far from the spot. Note also that in the spotless mode at the same current, the potential of the adjacent plasma is below the electrode potential and the electron sheath extends some 50 μm from the electrode.

3.3 Near-anode physics

The distribution of current density and electric field along the anode surface in the plane of symmetry $\phi = 0$ (the longitudinal cross section that passes through the centre of a spot),

line AB, is shown in figure 6. Plots are included for two different discharge currents. The current density has a large magnitude and is negative inside the spot, and turns positive outside. The spot behaves like a mini-cathode or, as one could say, operates as a unipolar glow discharge.

The direction of current density in the plane of symmetry, $ABED$, is shown in figure 7. For convenience, the distribution of the ions number density (the same as in figure 4b) is shown as well. The unipolar glow discharge is clearly seen.

The electric field at the anode in figure 6 is seen to be negative inside the spot and positive outside for 35 mA; it is negative everywhere for 1 mA. Directions of the electric field at the anode and of current density from the anode inside and outside the spot are summarized in table 1. Also shown are corresponding data for the (2D) spotless mode, where $E_z > 0$, $j_z > 0$ for all values of current.

Current	Within the spot	Outside the spot	Spotless mode
1 mA	$E_z < 0$, $j_z < 0$ (cathode)	$E_z < 0$, $j_z > 0$ (field reversed-anode)	$E_z > 0$, $j_z > 0$ (regular anode)
35 mA	$E_z < 0$, $j_z < 0$ (cathode)	$E_z > 0$, $j_z > 0$ (regular anode)	$E_z > 0$, $j_z > 0$ (regular anode)

Table 1. Physics of the near-anode region for the 3D solution.

4 Concluding remarks

Multiple solutions, describing different modes of current transfer in the near-anode region of a DC glow discharge and existing in the same range of discharge currents, were found for the first time: a 3D solution describing a self-organized pattern of anode spots and a 2D solution describing a spotless mode. A conventional glow discharge model was employed.

There are similarities between the patterns of anode spots and the patterns of spots on cathodes of arc and DC glow discharge: both are described by multiple steady state solutions and reveal azimuthal periodicity. On the other hand, the spots on the anode are different to the spots on the cathode in following ways: the solution describing the spotless mode does not contain a pronounced N-shaped current-voltage characteristic; no bifurcations were found in a wide range of currents, i.e., the anode spots were found to exist isolated from the 2D spotless mode. The anode spots are apparently related to the change in the sign of the near anode voltage.

Inside the spots the anode behaves like a mini-cathode, in that the sign of the current density and electric field is reversed. In other words, anode spot operates as a unipolar glow discharge.

The above-described physics is different from the physics revealed by the recent modelling [45, 46] of plasma balls, that form on anodes in contact with a low-pressure plasma and sometimes are termed anode spots. In particular, no double layers were found in the present modelling. One of the reasons of the difference is that the plasma balls appear not to be related to multiple solutions and therefore do not represent a self-organization phenomenon; note that size of plasma balls is larger than the width of the electrode. The difference in plasma pressure may contribute as well.

Bombardment on the anode by low-kinetic energy ions occurs inside the spots. An interesting hypothesis is that the ions incident on the anode contribute to or are responsible for the cancer-inhibiting effect reported in [25].

The modelling reported in this work should not be interpreted as an attempt to quantitatively describe parameters of anode spots. Merely, the aim was to prove the possibility of self-consistently describing self-organized anode spots on the basis of multiple solutions existing in the same range of discharge currents, which was achieved. A number of effects have to be taken into account in order to perform future quantitative modelling, among them being the complex plasma chemistry present in helium discharge, the nonlocality of electron energy, gas heating, neutral particle flow, and electron-electron collisions. Questions relating to the choice of the boundary conditions are also pertinent, as well as kinetic effects. Inspite of these caveats, one can expect that the findings of the existence of multiple solutions and the unipolar spots with a reversal of the near-anode potential would also be present in more detailed modelling.

5 Acknowledgments

The work was supported by FCT - Fundação para a Ciência e a Tecnologia of Portugal through the project Pest-OE/UID/FIS/50010/2013.

References

[1] O. Lehmann, Annalen der Physik **312**, 1 (1902).

[2] G. M. J. Mackay, Phys. Rev. Lett. **15**, 309 (1920).

[3] C. H. Thomas and O. S. Duffendack, Phys. Rev. **35**, 72 (1930).

[4] S. M. Rubens and J. E. Henderson, Phys. Rev. **58**, 446 (1940).

[5] K. G. Emeleus, Int. J. Electronics **52**, 407 (1982).

[6] K. G. Müller, Phys. Rev. A **37**, 4836 (1988).

[7] Ch. Maszl, J. Laimer, and H. Störi, IEEE Trans. Plasma Sci. **39**, 2118 (2011).

[8] V. I. Arkhipenko, T. Callegari, Y. A. Safronau, L. V. Simonchik, and I. M. Tsuprik, Plasma Sources Sci. Technol. **22**, 045003 (2013).

[9] T. Verreycken, P. Bruggeman, and C. Leys, J. Appl. Phys. **105**, 083312 (2009).

[10] N. Shirai, S. Uchida, and F. Tochikubo, Plasma Sources Sci. Technol. **23**, 054010 (2014).

[11] K. H. Schoenbach, M. Moselhy, and W. Shi, Plasma Sources Sci. Technol. **13**, 177 (2004).

[12] M. Moselhy and K. H. Schoenbach, J. Appl. Phys. **95**, 1642 (2004).

[13] Yu. D. Korolev and K. H. Schoenbach, in *Proc. XXVII ICPIG (Eindhoven, the Netherlands, July 2005)*, edited by E. M. van Veldhuizen (Eindhoven University of Technology, Eindhoven, 2005).

[14] N. Takano and K. H. Schoenbach, Plasma Sources Sci. Technol. **15**, S109 (2006).

[15] N. Takano and K. H. Schoenbach, in *Abstracts of the 2006 IEEE International Conference on Plasma Science* (IEEE, Traverse City, MI, USA, 2006) p. 247.

[16] B.-J. Lee, H. Rahaman, K. Frank, L. Mares, and D.-L. Biborosch, in *Proc. 28th ICPIG (Prague, July 2007)*, edited by J. Schmidt, M. Šimek, S. Pekárek, and V. Prukner (Institute of Plasma Physics AS CR, ISBN 978-80-87026-01-4, Prague, 2007) pp. 900–902.

[17] W. Zhu, N. Takano, K. H. Schoenbach, D. Guru, J. McLaren, J. Heberlein, R. May, and J. R. Cooper, J. Phys. D: Appl. Phys. **40**, 3896 (2007).

[18] B.-J. Lee, D.-L. Biborosch, K. Frank, and L. Mares, J. Optoelectron. Adv. Mater. **10**, 1972 (2008).

[19] K. H. Schoenbach and W. Zhu, IEEE J. Quantum. Electron. **48**, 768 (2012).

[20] W. Zhu, P. Niraula, P. G. C. Almeida, M. S. Benilov, and D. F. N. Santos, Plasma Sources Sci. Technol. **23**, 054012 (2014).

[21] W. Zhu and P. Niraula, Plasma Sources Sci. Technol. **23**, 054011 (2014).

[22] M. S. Bieniek, P. G. C. Almeida, M. S. Benilov, W. Zhu, and P. Niraula, in *43rd IEEE Int. Conf. Plasma Sci. (ICOPS 2016)* (2016).

[23] F. M. Gaysin and E. E. Son, *Electrophysical processes in the discharges of liquid and solid electrodes* (Urals State University, Sverdlovsk, 1989) in Russian.

[24] F. M. Gaysin, E. E. Son, and V. D. Shakirov, *Initialization and development of the volume discharge with liquid electrodes* (Polytechnicnical Institute, Moscow, 1990) in Russian.

[25] Z. Chen, S. Zhang, I. Levchenko, I. I. Beilis, and M. Keidar, Sci. Rep. **7**, 12163 (2017).

[26] R. S. Islamov, Phys. Rev. E **64**, 046405 (2001).

[27] R. S. Islamov and E. N. Gulamov, IEEE Trans. Plasma Sci. **26**, 7 (1998).

[28] Yu. Akishev, V. Karal'nik, I. Kochetov, A. Napartovich, and N. Trushkin, Plasma Sources Sci. Technol. **23**, 054013 (2014).

[29] V. A. Güntherschulze, W. Bär, and H. Betz, Z. Physik A **109**, 293 (1938).

[30] B. N. Klyarfel'd and N. A. Neretina, Sov. Phys. Tech. Phys. **5**, 169 (1960).

[31] F. G. Baksht, A. A. Kostin, N. K. Mitrofanov, and S. M. Shkol'nik, in *Proc. Conf. on Physics of Low-Temperature Plasma, Petrozavodsk, Russia, June 1995* (PGU, Petrozavodsk, RF, 1995) pp. 191–193, in Russian.

[32] F. G. Baksht, G. A. Dyuzhev, N. K. Mitrofanov, and S. M. Shkol'nik, Tech. Phys. **42**, 35 (1997).

[33] S. M. Shkol'nik, in *Encyclopaedia of Low-Temperature Plasmas*, Vol. 2, edited by V. E. Fortov (Nauka, Moscow, 2000) pp. 147–165, in Russian.

[34] G. Yang and J. Heberlein, Plasma Sources Sci. Technol. **16**, 529 (2007).

[35] J. Heberlein, J. Mentel, and E. Pfender, J. Phys. D: Appl. Phys. **43**, 023001 (2010).

[36] S. M. Shkol'nik, Plasma Sources Sci. Technol. **20**, 013001 (2011).

[37] J. P. Trelles, Plasma Sources Sci. Technol. **22**, 025017 (2013).

[38] J. P. Trelles, Plasma Sources Sci. Technol. **23**, 054002 (2014).

[39] L. M. Ivan, G. Amarandei, M. Aflori, M. Mihai-Plugaru, C. Gaman, D. Dimitriu, C. Ionita, and R. W. Schrittwieser, Acta Physica Slovaca **55**, 501 (2005).

[40] L. M. Ivan, G. Amarandei, M. Aflori, D. Dimitriu, and M. Sanduloviciu, IEEE Trans. Plasma Sci. **33**, 542 (2005).

[41] C. Charles, Plasma Sources Sci. Technol. **16**, R1 (2007).

[42] S. D. Baalrud, B. Longmier, and N. Hershkowitz, Plasma Sources Sci. Technol. **18**, 035002 (2009).

[43] B. Scheiner, S. D. Baalrud, B. T. Yee, M. M. Hopkins, and E. V. Barnat, Phys. Plasmas **22**, 123520 (2015).

[44] S. Chauhan, M. Ranjan, M. Bandyopadhyay, and S. Mukherjee, Phys. Plasmas **23**, 013502 (2016).

[45] B. Scheiner, S. D. Baalrud, M. M. Hopkins, B. T. Yee, and E. V. Barnat, Phys. Plasmas **23**, 083510 (2016).

[46] B. Scheiner, E. V. Barnat, S. D. Baalrud, M. M. Hopkins, and B. T. Yee, Phys. Plasmas **24**, 113520 (2017).

[47] M. S. Benilov, Plasma Sources Sci. Technol. **23**, 054019 (2014).

[48] A. Salabas, G. Gousset, and L. L. Alves, Plasma Sources Sci. Technol. **11**, 448 (2002).

[49] G. J. M. Hagelaar, F. J. de Hoog, and G. M. W. Kroesen, Phys. Rev. E **62**, 1452 (2000).

[50] P. G. C. Almeida and M. S. Benilov, Phys. Plasmas **20**, 101613 (2013).

[51] R. N. Franklin, *Plasma Phenomena in Gas Discharges* (Clarendon Press, Oxford, 1976).

[52] M. S. Bieniek, P. G. C. Almeida, and M. S. Benilov, J. Phys. D: Appl. Phys. **49**, 105201 (2016).

[53] J. Mentel and J. Heberlein, J. Phys. D: Appl. Phys. **43**, 023002 (2010).

[54] T. Hoebing, A. Bergner, P. Hermanns, J. Mentel, and P. Awakowicz, J. Phys. D: Appl. Phys. **49**, 155504 (2016).

Figure captions

Figure 1. Schematic of calculation domain. AD is the axis of symmetry. Oval at point G represents location of a spot.

Figure 2. Near-anode voltage drop for a wide range of currents. 2D and 3D solutions are shown with schematics that indicate a characteristic distribution of electron number density on the anode.

Figure 3. Electron number density on the surface of the anode. 3D solution, $I = 10\,\mathrm{mA}$.

Figure 4. Distributions in the plane of symmetry passing through the spot center. $I = 1\,\mathrm{mA}$. a) Electron number density. b) Ion number density. c) Electrostatic potential.

Figure 5. Number density of ions (solid) and electrons (dashed) for $I = 35\,\mathrm{mA}$ and $I = 0.1\,\mathrm{mA}$. Reduced electric field (dotted) for $I = 35\,\mathrm{mA}$. Plot made along the line GH in figure 1.

Figure 6. Distribution of axial current density and axial electric field on the surface of the anode in the plane of symmetry passing through the spot center. Large negative values of electric field are not shown.

Figure 7. Distribution of the number density of ions in the plane of symmetry passing through the spot center. Arrows: direction of the current density vector. $I = 1\,\mathrm{mA}$.

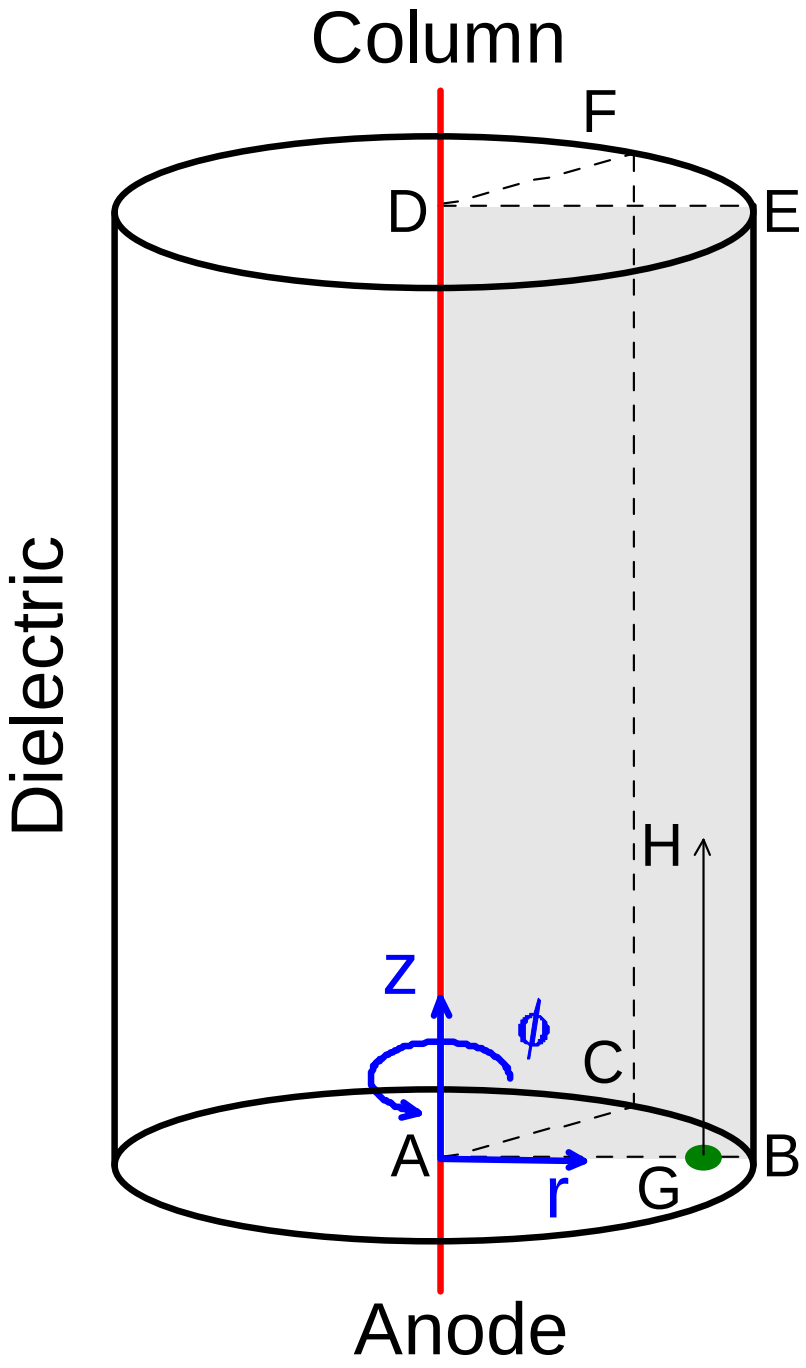

Figure 1. Schematic of calculation domain. AD is the axis of symmetry. Oval at point G represents location of a spot.

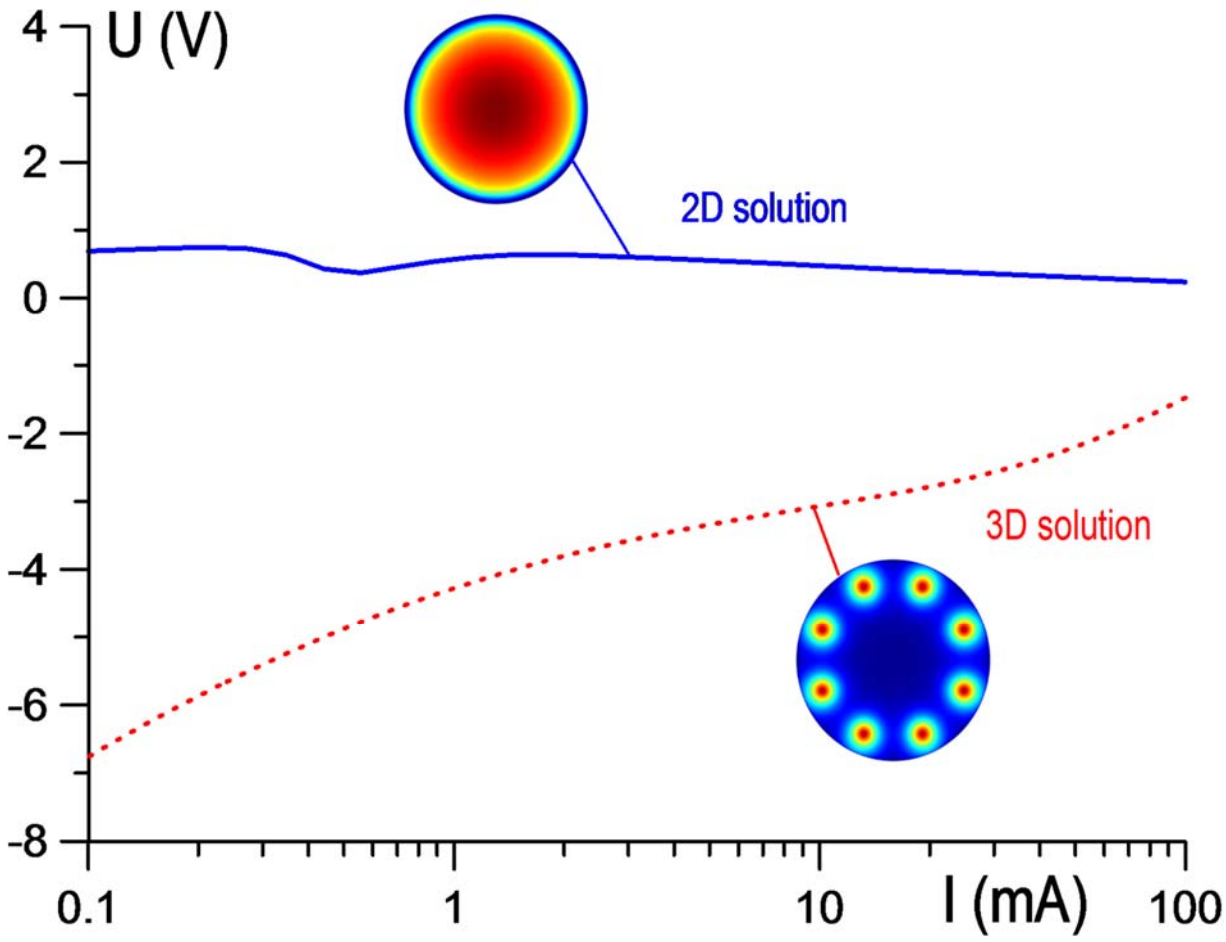

Figure 2. Near-anode voltage drop for a wide range of currents. 2D and 3D solutions are shown with schematics that indicate a characteristic distribution of electron number density on the anode.

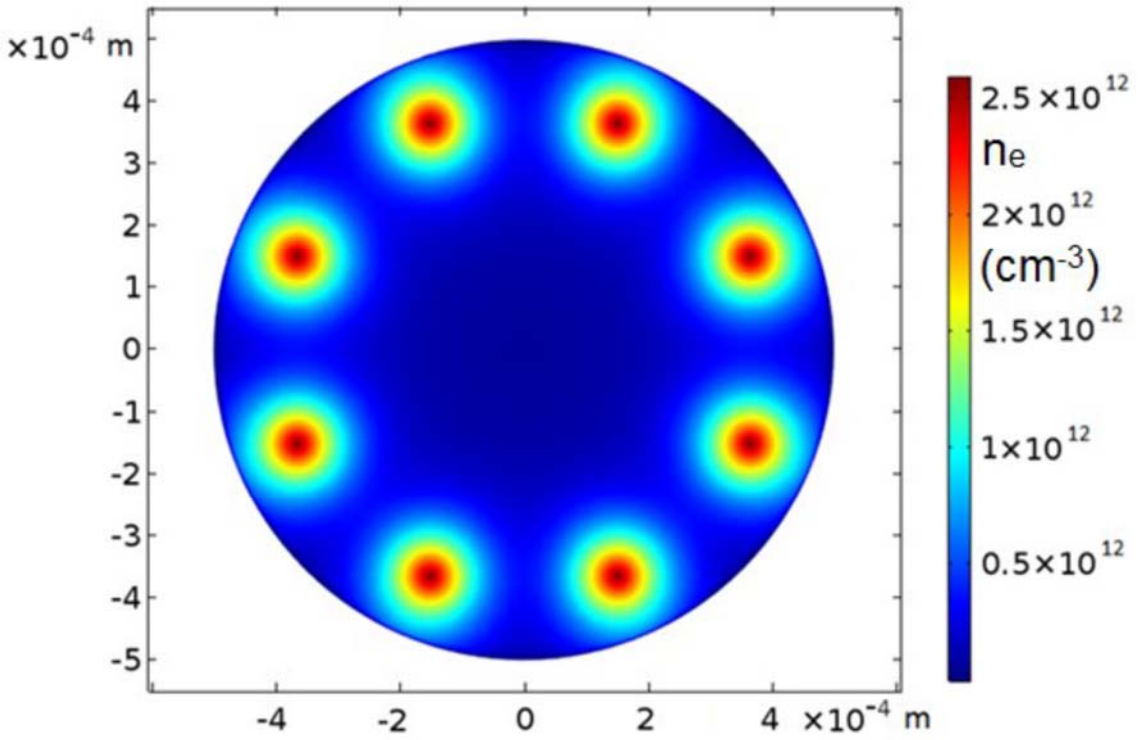

Figure 3. Electron number density on the surface of the anode. 3D solution, I = 10 mA.

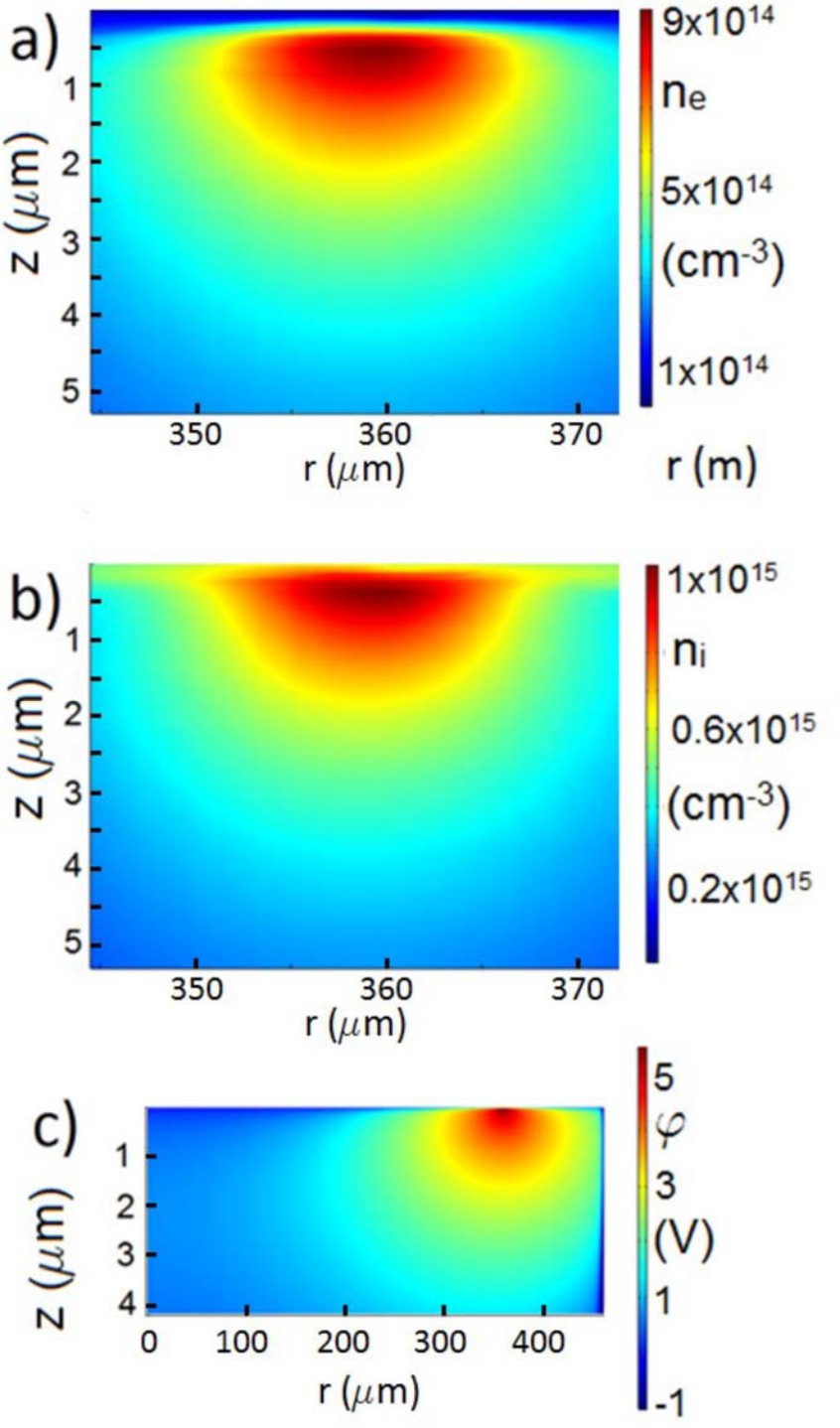

Figure 4. Distributions in the plane of symmetry passing through the spot center. I = 1 mA. a) Electron number density. b) Ion number density. c) Electrostatic potential.

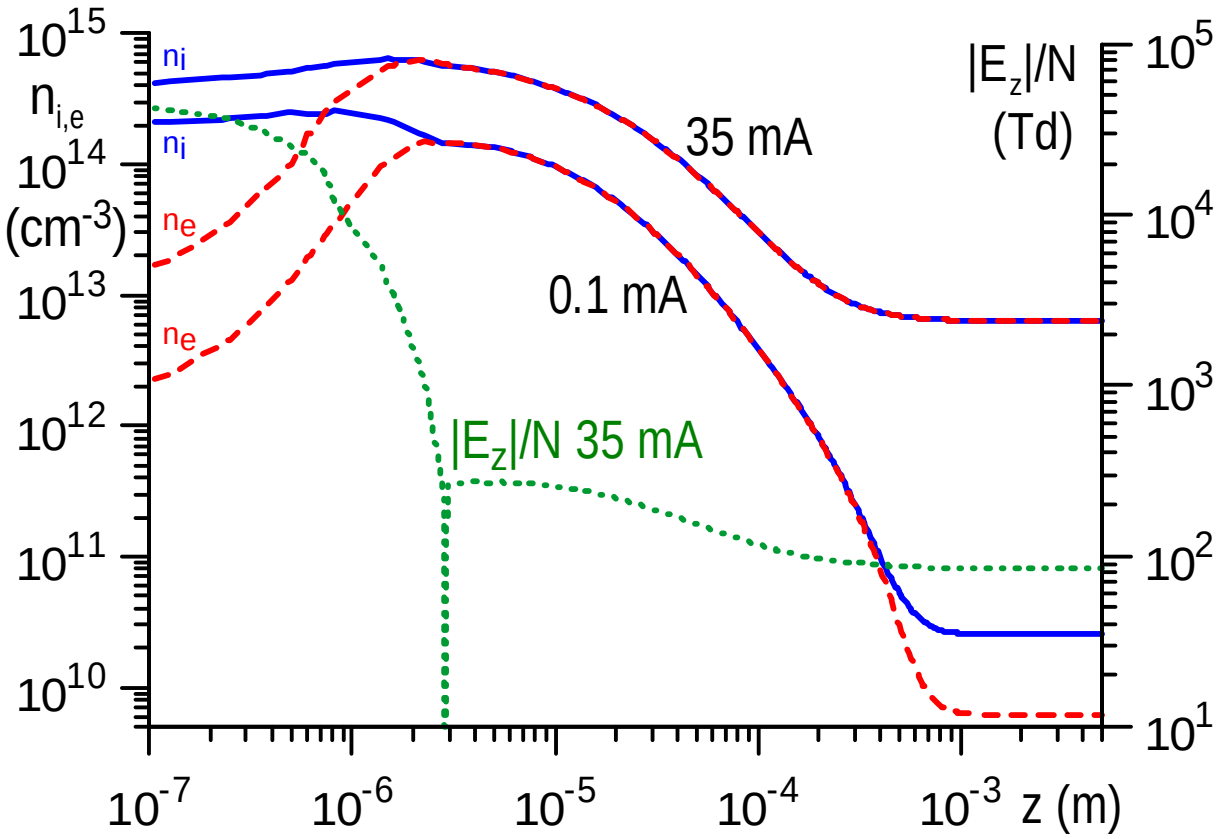

Figure 5. Number density of ions (solid) and electrons (dashed) for I = 35 mA and I = 0:1 mA. Reduced electric field (dotted) for I = 35 mA. Plot made along the line GH in figure 1.

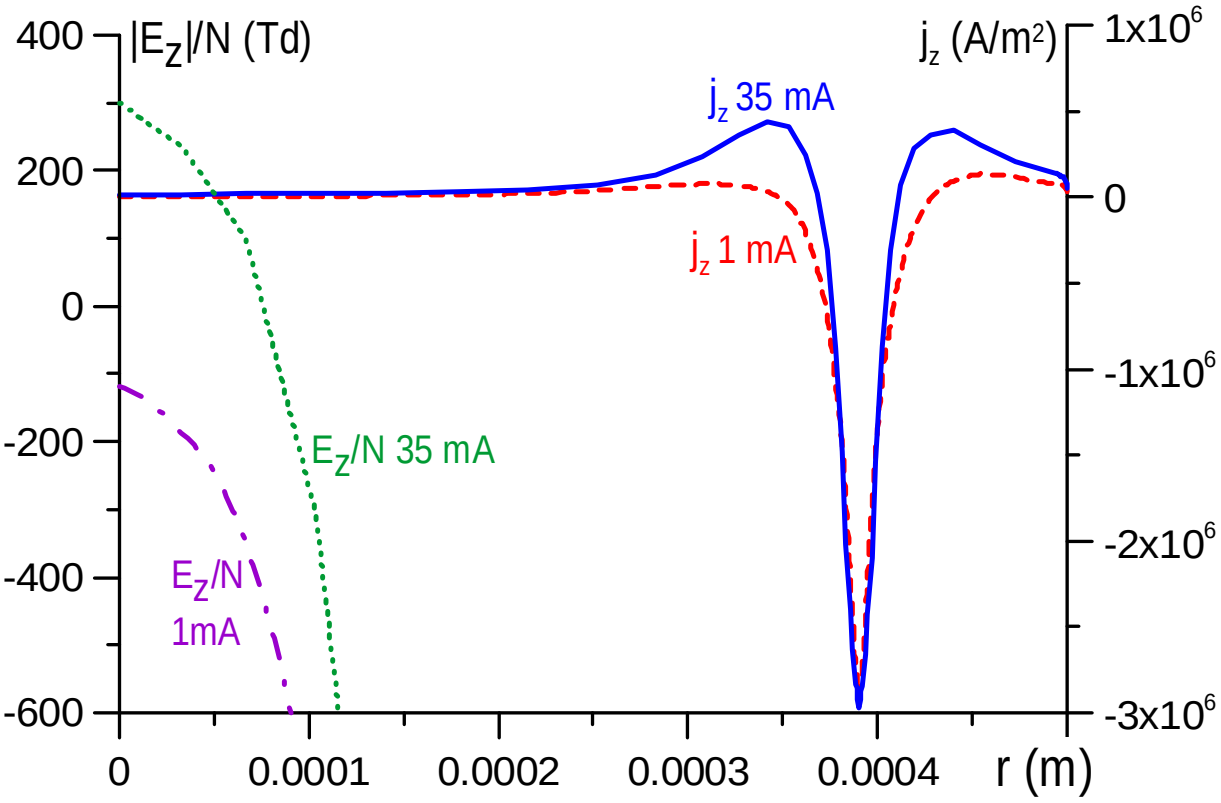

Figure 6. Distribution of axial current density and axial electric field on the surface of the anode in the plane of symmetry passing through the spot center. Large negative values of electric field are not shown.

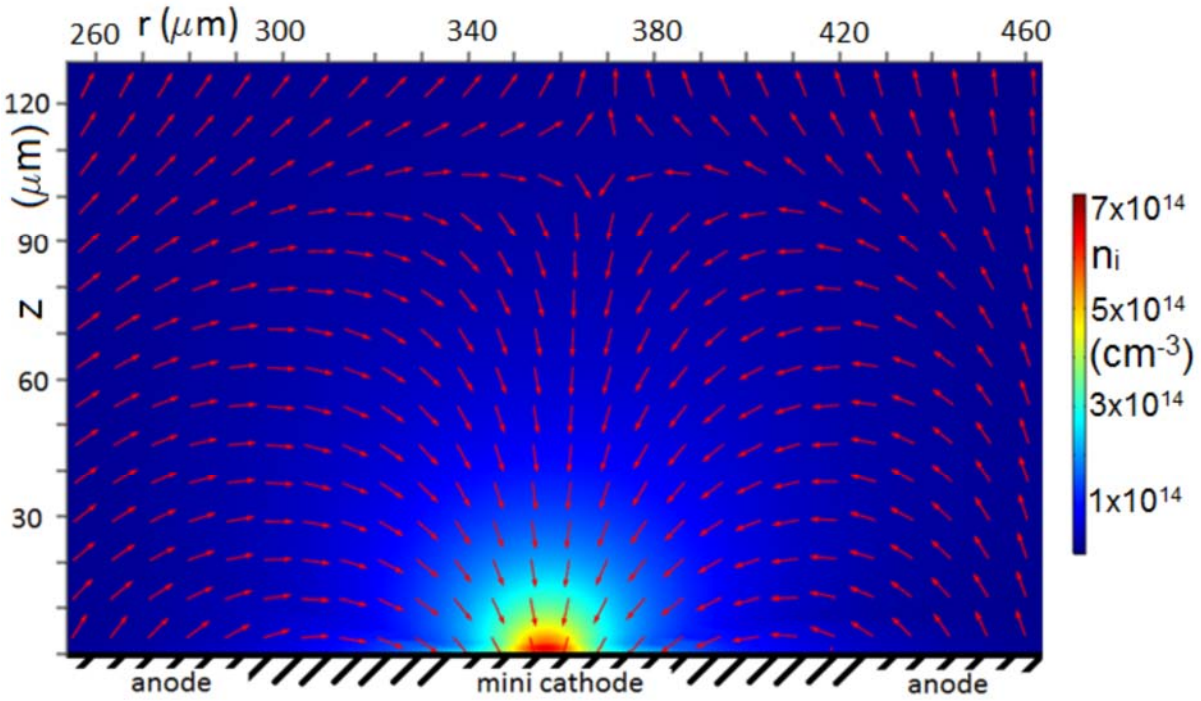

Figure 7. Distribution of the number density of ions in the plane of symmetry passing through the spot center. Arrows: direction of the current density vector. I = 1 mA.